HYBRID NATURAL-FIBRE COMPOSITE SANDWICH PANEL WITH NANOCOMPOSITE REINFORCEMENT FOR FLATWISE COMPRESSION AND VIBROACOUSTIC APPLICATIONS

R. Palumbo[1*], F. Scarpa[2], D. Ivanov[2], O. Bareille[3], C. Droz[3], M. Ichchou[3]

[1] European Space Agency (ESA), ECSAT - European Centre for Space Applications and Telecommunications, United Kingdom
[2] Bristol Composites Institute (ACCIS), University of Bristol, United Kingdom
[3] Vibroacoustics Complex Media Research Group (LTDS), Ecole Centrale de Lyon, France
* Corresponding author (rita.palumbo@esa.int)

Keywords: Natural fibres, Nanocomposites, Sandwich panels, Vibration damping

ABSTRACT

This paper illustrates the development of a novel sandwich panel for vibroacoustic applications by using novel materials as passive damping mechanisms. A flax-fibre composite is adopted for lattice core and skins. Carbon-nanotube reinforced viscoelastic inserts are embedded in critical locations within the lattice to further increase its vibration damping and potentially increase its strength. Restrictions to the mass added by the inserts are imposed to preserve the lightweight advantage of the panel. Quasi-static analyses are carried out to guarantee good-quality structural performances. The flatwise compression characterisation of bare- and reinforced cores shows that both configurations outperform comparable benchmark cases in terms of normalized stiffness and strength. The reinforced configuration presents 24.5% higher normalized strength compared to the bare panel. Two different types of vibration tests are performed. Results of out-of-plane vibration transmissibility tests show that the bare configuration outperforms that with inserts due to Coulomb dry friction effects. The CNT reinforced panel offers the highest viscoelastic damping in free vibrations conditions.

1 INTRODUCTION

Sandwich panels have been extensively used during the last eighty years due to the high stiffness-to-weight ratio they provide. Such characteristic is conferred by their two face skins separated by a low-density core, which can traditionally be either a porous layer or a cellular structure.
High-density rectangular lattices for cellular cores are preferable to hexagonal ones for shock loads as they combine resistance to crushing and energy absorption with in-plane (IP) stretching strength [1, 2, 3]. Rectangular lattices are easy to manufacture, which makes them ideal to experiment novel materials as core platforms. The mechanical performances of rectangular cell topology have been extensively reported in open literature, especially in terms of out-of-plane (OOP) strength and response to impact [1-6]. Most materials traditionally used in sandwich panels are fossil-based (aluminum, Nomex, Kevlar, glass- or carbon-fibre composites). Natural fibres are studied not only for their low environmental impact, but also for the higher energy dissipation and recyclability. They are already widely adopted in secondary load bearing applications like automotive interiors and non-critical packaging [7, 8, 9]. The challenge is to make them applicable to load-bearing structures.

In this work, a flax fibre composite is adopted to build sandwich panels core and skins. Viscoelastic inserts are embedded within the core to increase its vibration damping with low weight penalty [10, 11, 12]. The viscoelastic material adopted for the inclusions is a Carbon-nanotube (CNT) reinforced resin. CNTs are renowned for providing high energy absorption due to the stick-slip mechanism dissipating energy by interfacial friction between the CNT's outer surface and the surrounding polymer [13, 14, 15]. By placing the inserts at these critical locations, the core strength is also expected to increase [16]. The lattice topology is shown in Figure 1(a). Figure 1(b) and (c) represent the resin deposition by means of a 3D printed injection device. A CNT insert is shown in Figure 1(d).

This paper describes the development of a novel natural fibre sandwich panel with distributed viscoelastic inserts for vibration applications and structural integrity. The OOP compression strength is one of the key metrics to verify for structural integrity [17] and a paramount investigation for quality assurance. Therefore, the paper first focuses on the strengthening effect provided by the inserts in quasi-static flatwise compression tests, hereby verifying that the core provides comparable performance to analogous cases of lab-scale cores available in open literature. Secondly, it shows the vibration characterization of sandwich panels specimens with and without inserts.

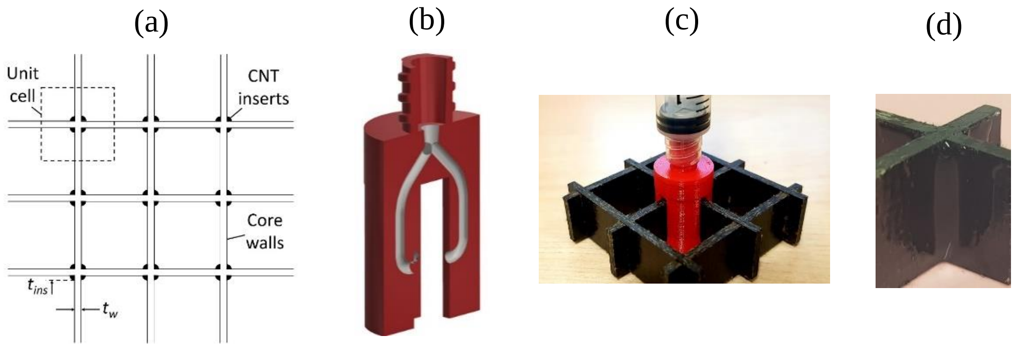

Figure 1: (a) Reinforced lattice topology. (b) 3D-printed injection mould for CNT-resin deposition—AutoCAD 2017. (c) CNT-resin injection mechanism. (d) Viscoelastic insert at walls junction.

2 MATERIALS MANUFACTURING AND CHARACTERIZATION

The lattice walls consist of a flax fibre and poly(furfuryl alcohol) (PFA) composite. PFA is a relatively new introduction, mainly used as matrix in natural-fibre composites. It is a bio-derived resin made from crop waste, hence often used with natural reinforcements to develop bio-composites [21]. The prepreg adopted in this study is Evopreg PFC-flax, Biotex flax 400 g/m^2 2x2 twill (Composites Evolution Ltd, UK), 50% resin weight fraction and 46% theoretical fibre volume fraction.
The viscoelastic inserts resin is obtained by mixing Nanocyl SA EPOCYL™ 128-06 with Super Sap CLV Epoxy Bio Resin (SS CLV - Entropy Resins, Gugeon Brothers Inc, MI). EPOCYL™ 128-06 is a masterbatch of Bisphenol-A (Bis-A) epoxy resin with high concentrations of multi-walled CNTs. SS CLV provides a clear, low-viscosity bio-derived epoxy system, suitable to the present application.

2.1 Materials manufacturing methods

The composite laminates consist of four-layer laminates. The prepreg is analysed by Differential Scanning Calorimetry to determine its curing temperature. Laminates are cured in autoclave at 140℃ 6.9 bar, with heat ramp of 0.5℃/min and dwell at 80℃ for 1.5 hours. The laminate thickness is 2.3 mm (standard deviation, STD DEV, 0.05 mm; Coefficient of Variation, CV, 2.08%).

The EPOCYL paste is diluted in the SS CLV resin with dilution factor of 6. The mixing is performed using a Silverson's high shear rotor/stator laboratory mixer at a speed of 50 rpm. The final CNTs concentration is 0.477 wt%. Pristine and CNT resins are cured at room temperature in 24 hours.

2.2 Mechanical characterization

2.2.1 Evopreg PFC-flax

Tensile tests are performed according to ASTM D3039/D3039M—17 on batches of samples with fabric orientation 0/90° and ±45°. The testing machine is a 10 kN load cell Shimadzu, crossbar displacement rate 2 mm/min. Emery cloth is used for gripping the samples as a substitute to end tabs. Strains are measured with Imetrum Limited's video-gauge extensometer - Digital Image Correlation

Video Gauge™. The Poisson's ratio is evaluated by linear regression of the strains in the linear range. The IP shear modulus is evaluated as per ASTM D3518/D3518M from tensile tests on samples with fabric at ±45°. Data is processed in MATLAB with the Chauvenet criterion. Results are reported in Table *1* and Figure 2.

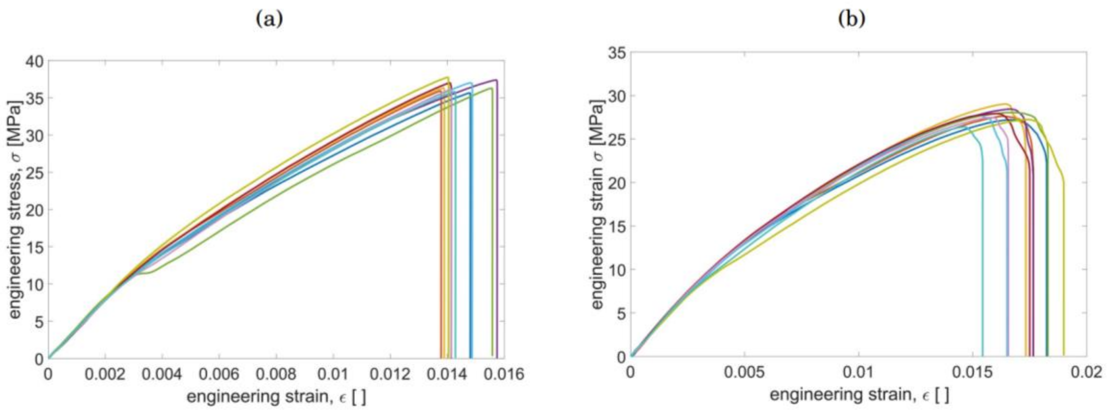

Figure 2: Stress-strain curves of Evopreg PFC-flax specimens. Fibres at (a) 0/90◦ and (b) ±45◦.

		Mean	STD DEV	CV
Fibres 0/90°	Young's Modulus [GPa]	3.69	0.111	3.01%
	Tensile Strength [MPa]	33.5	0.652	1.95%
	Yield Stress [MPa]	22.2	0.977	4.40%
	Elongation [%]	1.45	0.0691	4.76%
	Poisson's Ratio [ ]	0.336	0.114	33.9%
	Shear Modulus [GPa]	0.877	0.0601	6.86%
Fibres ±45°	Young's Modulus [GPa]	2.69	0.092	3.42%
	Tensile Strength [MPa]	25.4	0.660	2.60%
	Yield Stress [MPa]	17.8	0.833	4.68%
	Elongation [%]	1.62	0.0793	4.89%

Table 1: Summary of experimentally measured mechanical properties of Evopreg PFC-flax laminates cured with vacuum-bagging/autoclave techniques.

2.2.2 Pristine and CNT-resin

The characterization of the CNT-resin is performed according to ASTM D638-14 by testing dumbbell-shaped specimens of the resin cured at room temperature. Experimental values are compared to analytic predictions according to the model of Halpin and Tsai [19] with Thostenson correction [20] for quality control. Results are presented in Figure 3. The measured CNT-resin Young's Modulus is 1.99 GPa (CV 3.29%), while the pristine resin's is $E_{pristine}$=1.82 GPa. With this value of $E_{pristine}$ and w_{NT}=0.477 wt%, the analytic model predicts an effective Young's Modulus of 1.92 GPa. This estimation is close to the measured value – 1.99 GPa – showing 3.9% error between experimental and analytic data.

3 DESIGN AND MANUFACTURING OF THE SANDWICH PANEL

The square-cell lattice has unit cell width l = 20 mm, height h_{core}= 15 mm and walls thickness t_w = 2.3 mm. The walls are grooved strips with fibres at 0/90◦, resulting in a relative density of $\rho/\rho_s = (2t_w l - t_w^2)/l^2$ = 0.23. Skins are cut from laminates with fibres at 0/90◦ and glued to the core with pristine SS CLV resin. For the inserts design, gravity affects its shape once the resin has been deposited and before it cures completely, resulting in a non-uniform distribution approximated by a hyperbolic shape (Figure 4). The insert design space is determined by setting a limit of 5% to the percentage of added mass. By considering an equivalent cylindrical insert, its volume results in $\pi r^2 h_{core} = 79.6\ mm^3$, corresponding to a nominal radius $r = 1.3\ mm$.

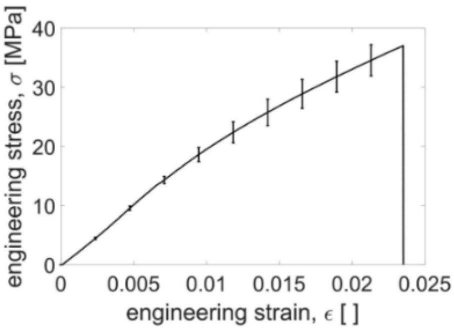

Figure 3: Tensile tests curves of CNT SS CLV Epoxy Bio-resin (mean curve with STD DEV).

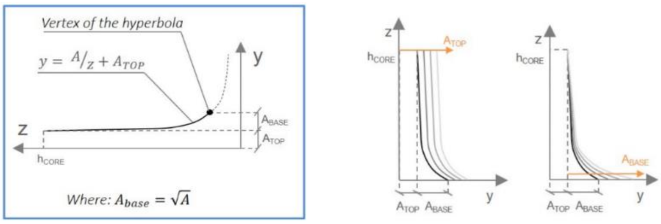

Figure 4: Qualitative drawing of the insert's hyperbolic geometry.

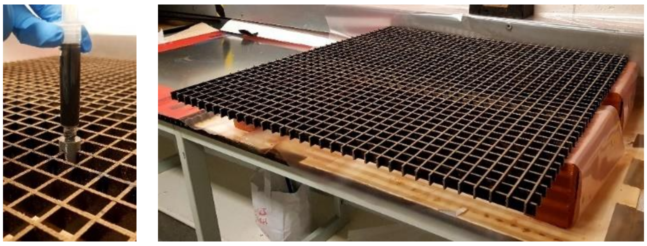

Figure 5: Large-scale sandwich panels: CNT-reinforced resin injection at walls junction areas. (a) Injection process; (b) final reinforced core.

Inserts are manufactured by means of a 3D printed injection device applied to the tip of a medical syringe—Figure 1 and Figure 5. A probabilistic design analysis is performed to check the significance of the insert's geometric uncertainties to the unit cell global properties. It is verified that the deviation of the insert's shape from cylindrical is only marginally significant to the global properties.

4 QUASI-STATIC CHARACTERIZATION

Highly damping materials like natural fibres might decrease the core mechanical efficiency because of their lower stiffness and strength compared to traditional core materials [7, 8, 9]. OOP compression tests are performed in the following sections to evaluate the compression strength. The latter is one of the key metrics to assure for structural integrity [17] and a paramount investigation for quality assurance.

4.1 Methods

Quasi-static flatwise compression tests are performed by means of an Instron 600DX testing machine. For each configuration, five specimens with 100 mm x 100 mm transverse area and non-stabilized faces (*i.e.*, no skins) are tested. Tests are performed according to the ASTM C365/C365M-16. The linear elastic range used for the evaluation of the Compression Modulus is $\varepsilon \in [0.6 \div 1.6]\%$ for the bare configuration, $\varepsilon \in [2 \div 3]\%$ for the reinforced. The strain displayed in the $\sigma(\varepsilon)$ curves is the engineering strain, $\varepsilon = \delta / h$, being $h = h_{core}$ the initial core height. Finally, all data undergoes the Chauvenet criterion [18] to define the outliers in the evaluation of the statistic properties.

4.2 Results

Figure 6 displays the compression tests results. Bare and reinforced lattices fail by material fracture at 147 and 183 kN, respectively. The reinforced core shows 24.5% higher failure stress compared to the bare one, with a 25% increment of relative density. The curves do not start from zero most likely due to manufacturing factors and imperfect flatness levels of the specimens which cause the system to undergo an initial adjustment phase as load is applied.

The OOP mechanical properties are compared to other literature cases in the performance charts in Figure 7. Since the charts contemplate different types of lattices, stiffness and stress are normalized to the Tensile Modulus of core walls material, E_s. This is a conventional method for presenting results in performance charts to consider the different materials of the cellular structures [19].

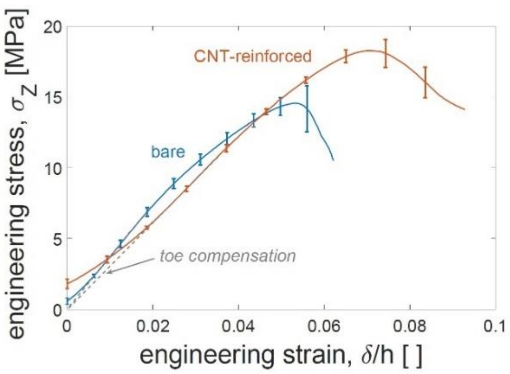

Figure 6: Flatwise compression results, $\sigma(\varepsilon)$ mean curves with STD DEV.

Following, a short review of the benchmark cases considered for comparison. Zuhri et al. [20] investigated the compression characteristics of square- and triangular-cell honeycomb cores reinforced with flax fibres in Polypropylene (PP) and Poly(lactic acid) (PLA) polymers. Stocchi et al. [21] examined hexagonal-cell honeycomb cores of jute fibres in vinyl ester (VE) matrix with different cell dimensions. Côté et al. [2] evaluated the compression behaviour of metallic honeycombs with square cells and different height-to-length (H/L) values. Hayes et al. [5] examined the mechanics of linear cellular alloys, considering different grades of maraging steels and several cell array configurations. In [19] the transverse properties of Kirigami zero-ν Polyether ether ketone (PEEK) honeycombs were explored. Del Broccolo et al. [22] performed a comparative study between PEEK hexagonal (HEX) and AUXHEX configurations (a type of topology conferring zero-ν behaviour).

The flax/PFA lattices appear to possess outstanding performances compared to the other literature cases. Both bare and reinforced panels perform remarkably better than the other cases. The normalized failure stress is higher for the flax/PFA cores than flax cores with thermoplastic matrix (PLA and PP) and similar relative densities. Likewise, flax/PFA cores perform better than the Jute lattices with thermoset resin (VE). Hence, it is possible to ascertain that the PFA resin might play an important role in the unusually great compression characteristics of the flax/PFA cores presented in this work.

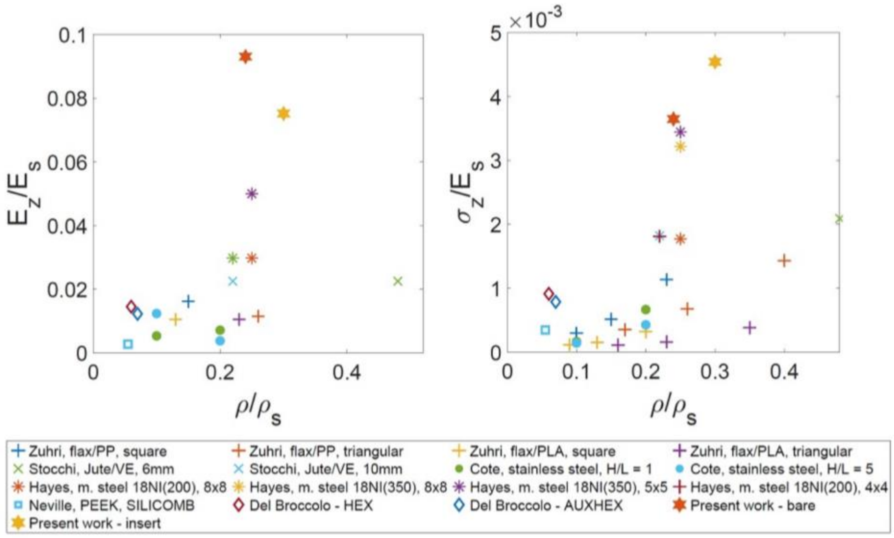

Figure 7: Quasi-static flatwise compression performance charts: stiffness and strength compared to open-literature cases. Normalization with respect to walls solid Tensile Modulus.

5 VIBRATION CHARACTERIZATION

Two different types of dynamic tests are performed: OOP vibration transmissibility tests on small-scale sandwich panels and free vibration tests on large-scale panels. The following sections explore methods adopted for numerical predictions and experimental validation, followed by the results.

5.1 Methods

5.1.1 OOP vibration transmissibility

Transmissibility tests consist of shaker-excited SDOF systems which provide accurate measurements of amplitude and phase over a frequency range [23]. The specimen is subjected to excitation at its base by an electromagnetic shaker and the acceleration is measured at the base and top of the specimen - Figure 8. Other than the specimen mass, m, the acceleration sensor and any weight added on the sample must be accounted for, M. The resonance peak amplitude, A, is determined as the ratio of the measured accelerations, $A = |X/X_0|$, X being the free response measured at the top of the specimen and X_0 that measured at the base. The modulus at the resonance frequency ω_R and the loss factor η are evaluated as:

$$k = \left(M + \frac{m}{3}\right)\omega_R^2 \tag{1}$$

$$\eta = \frac{1}{\sqrt{A^2 - 1}} \tag{2}$$

5.1.1.1 Numerical simulations

FE simulations of the transmissibility tests are performed in ANSYS Mechanical APDL R15 on a unit cell model (average element size of 1.25 mm). Mechanical properties of materials are assigned as per results of materials characterization. The damping is assigned as internal material property with the values estimated through DMA tests by averaging tanδ values at room temperature and 1 Hz frequency. For the Evopreg PFC-flax, tanδ = 2ζ = η = 0.0290 (STD DEV 0.0061) whereas for the CNT-resin tanδ = 2ζ = η = 0.0461 (STD DEV 0.0057). Perfect bonding is assumed between parts. To simulate the surrounding structure, sliding boundary conditions are applied to the cell edges. The nodes at the top of the cell are linked via master-slave multi-point constraints (MPC) and the mass M is applied to the MPC master node through a MASS21 element. A second MPC connection is applied to the base nodes and a harmonic displacement between 0 and 10 kHz is applied to its master node.

5.1.1.2 Experimental tests

Figure 9 and Figure 10 show the setup of vibration transmissibility tests. The instrumentation consists of Lyng Dynamic System (LDS) electromagnetic shaker and power amplifier; Support table with Newport I-2000 Vibration Isolation Stabilizers; Four-channel signal acquisition module, National Instruments (NI) 9234 (accelerations: analog to digital signals); Voltage output module, NI 9263 (excitation: digital to analog signal); Kistler signals conditioning system for accelerations; Computer for controlling the shaker and processing output data. The sandwich panel specimens have IP dimension 50.8 mm x 50.8 mm. The frequency range is set to 0 − 6000 Hz with sampling frequency of the input signal set to 25600 Hz. Superglue is adopted to attach all the components - i.e., the specimen to base plate and mass, one accelerometer to the base plate, one accelerometer to the top mass. Gaussian noise with amplitude 1 V and a mass of 129 gr are adopted. Signal processing is executed in MATLAB. For the stepped-sine excitation, signals are filtered with a band-pass Hamming filter of 30th order. The Frequency Response Function is computed at each single frequency in terms of single-sided spectrum.

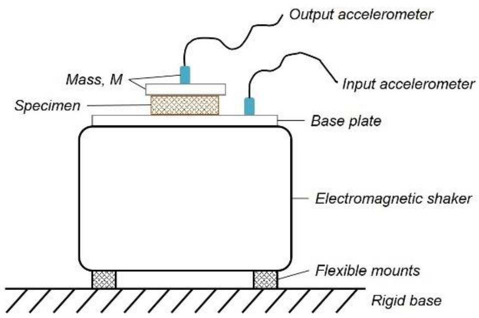

Figure 8: Schematic drawing of shaker excited SDOF system tests (OOP vibration transmissibility).

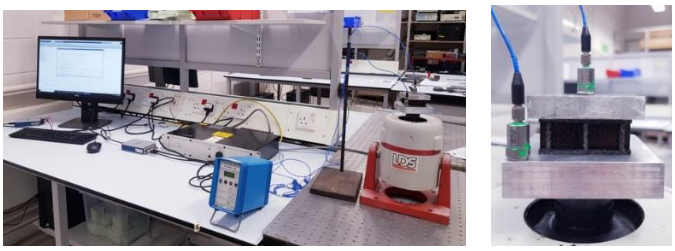

Figure 9: Setup of vibration transmissibility tests and detail of the specimen configuration.

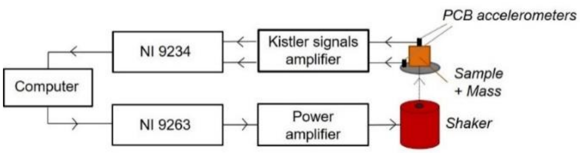

Figure 10: Schematic representation of vibration transmissibility test experimental setup.

5.1.2 Free vibration tests of large-scale sandwich panels

Free vibration tests are performed on bare and reinforced large-scale panels (IP area 680 mm x 680 mm) at the Ecole Centrale de Lyon facilities, Laboratory of Tribology and Systems Dynamics. The frequency response function (FRF) is evaluated numerically and experimentally. An FRF is a representation of the relationship between input and output of two points in a system:

$$\mathrm{H(f)} = \frac{Y(f)}{X(f)} \tag{3}$$

Y(f) and X(f) are respectively the system output and input in the frequency domain, that is the Fourier Transform of the corresponding signals in time domain, X(t) and Y(t).

5.1.2.1 Numerical assessments

The FE models are based on the ones described in section 5.1.1.1. A courser mesh used in this case to reduce the computational cost due to the large model dimensions. The unit cell is shifted along the two IP orthogonal axes 34 times to obtain the final panel (total number of unit cells: 1156). The bare cell model has 238 nodes, the whole panel 203188. The reinforced cell model has 398 nodes, the whole panel 370196. Simulations are run in free-free boundary conditions. Harmonic analyses are performed in the frequency range 0−1000 Hz with 200 substeps by applying a unitary cyclic excitation load at the center of one of the skins and reading the cyclic response at the central node of the opposite skin. The load amplitude is maintained the same for all substeps (stepped load). Results of these analyses are used to define the number of experimental acquisition points. Usually, 6 to 10 points per wavelength are necessary to capture a sine wave, so the grid is such to have 6 to 10 points per wavelength at the highest frequency investigated, that is 1000 Hz.

5.1.2.2 Experimental investigations

The sandwich panels are hung to a support structure to resemble free-free boundary conditions. The instrumentation consists of three groups of equipment - Figure 11 and Figure 12. **Power input**: Controller-Dynamic Signal Analyzer; Data Physics Power Amplifier; Data Physics Modal Shaker (cut-off 3000Hz); 1 BNC connector. **Transducer**: Mechanical Impedance Sensor PCB Piezotronics; ICP signal conditioner; 2 Microdot cables and 2 BNC connectors. **Frequency response measurement**: Polytec Scanning Vibrometer laser; Reflective paper - 19.6 gr, 0.3% added mass to each panel. The acquisition grid consists of 20x21 points, marked with reflective paper. Pseudo-random noise excitation with signal amplitude 0.5 V is used and 40 averages are made for each acquisition point. The frequency range is 0−1000 Hz with 1600 frequency lines (sample frequency 2.56 kHz, resolution 625 mHz and sample time 1.6 seconds). The FRF, H1(f), is estimated as:

$$\mathrm{H1(f)} = \frac{S_{xy}(f)}{S_{xx}(f)} \tag{4}$$

where S_{xy}(f) is the Cross Spectral Density in the frequency domain of X(t) and Y(t) and $S_{xx}(f)$ the Auto Spectral Density in the frequency domain of X(t). Data is processed in MATLAB and a Savitzky-Golay digital filtering [24] is applied. The FRF is measured as velocity over force from the vibrometer and force measurements. Finally, the loss factor is evaluated with the Half-Power Method [25] as

$$\eta = \frac{\Delta\omega}{\omega_r} = \frac{\omega_2 - \omega_1}{\omega_r} \tag{5}$$

ω_r is the resonance frequency and $\omega_{1,2}$ are the values corresponding to $A = A_{peak}/\sqrt{2}$.

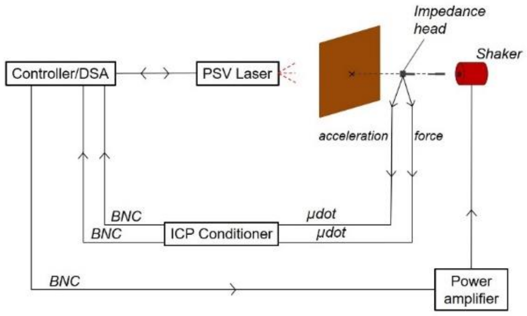

Figure 11: Frequency response experimental analysis: schematic drawing of measurement setup.

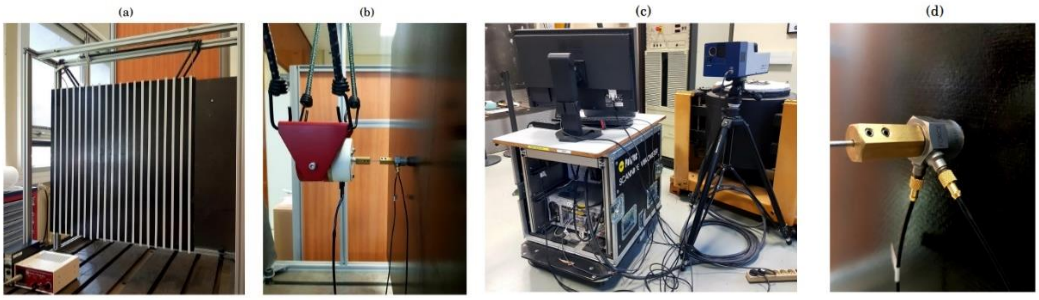

Figure 12: Frequency response analysis experimental setup. (a) Sandwich panel; (b) Shaker applied to the panel; (c) Scanning Vibrometer laser; (d) Mechanical Impedance Sensor PCB Piezotronics.

5.2 Results

5.2.1 OOP vibration transmissibility

Figure 13 shows the results of transmissibility analyses. The bare panel has remarkably lower peak of transmissibility than that with inserts. This due to Coulomb dry friction phenomena acting in the bare panel between interlocking walls, causing high levels of energy dissipation.

The CNT-resin at the wall junctions in the reinforced panel prevents any Coulomb dry friction phenomena: in this load case, the viscoelastic damping provided by the inserts does not give a relevant contribution to the overall damping of the panel, which is dominated by structural damping instead. Figure 13 also shows the numerical results, which for the reinforced configuration agree with the experimental ones. For the bare panel instead, friction damping is not considered in the FE model, which is hence tuned to the experimental results by assigning a value of material damping to the entire model. The latter is found from the experimental peak of transmissibility (0.0725).
Table 2 summarizes values of resonance frequencies, peak of transmissibility and loss factor. The loss factor is evaluated according to Eq. 2 from the peak amplitude. Table 2 also shows the Complex Stiffness amplitude as per Eq. 1, where the mass of bare and reinforced panels is 30.009 gr and 31.142 gr, respectively. The Young’s Modulus is calculated by applying the classic relation between Young’s Modulus and stiffness for purely axial deformation, $K = EA/H$.
Loss factor values are also estimated by the Half Power Method, Table 3. For the numerical curves, both methods give comparable results, whereas for the experimental curves the Half-Power Method loss factor is about half the peak amplitude method value. This is probably due to experimental factors, as in the experimental curves there is a steep drop after the peak. In the present case, it is hence more reliable to evaluate the loss factor through the peak amplitude method.

5.2.2 Free vibration

Figure 14 shows good agreement between numerical and experimental data. Figure 15(a) shows the average FRF spectrum. In Figure 15(b) and Figure 15(c), the Half-Power Method is applied to the first two resonance peaks of the average spectrum. Table 4 summarizes resonance frequencies and loss factor values. The contribution to damping given by the inserts is evident: at the first peak, the loss factor is 8.33% higher for the CNT panel, for the second peak is 15.3% higher. At low frequencies, a sandwich structure behaves as a homogeneous panel and is controlled by the total section bending stiffness [26]. Therefore, the CNT panel provides higher loss factor due to the inserts damping contribution.

6 CONCLUSIONS

This paper brought together different aspects concerning the development of a sandwich panel for vibroacoustic applications. The material adopted for core walls and skins is a flax bio-composite in PFA resin. Viscoelastic inserts made of CNT-resin are designed to provide maximum additional mass of 5%. Materials are characterized through mechanical and dynamic tests, and a manufacturing procedure is successfully developed for small- and large-scale panels. The lattices structural integrity is verified via OOP compression tests, and results are compared to benchmark cases from open literature. The bare flax/PFA core developed in this work features the highest normalized stiffness, while the CNT-configuration offers the highest normalized compression strength. Dynamic tests results suggest that different mechanisms intervene to dissipate mechanical energy depending on the boundary conditions and load cases. When the panels are excited uniformly OOP, the bare configuration dissipates mechanical energy by Coulomb dry friction acting at the wall junction areas. In this case, experimental results suggest that the contribution of internal material damping to the overall loss factor is small compared to the structural damping. Conversely, when the sandwich panels are free to deform with flexural bending deformation, the CNT-insert contribution to vibration damping is evident as the main energy dissipation mechanism is given by internal material damping.

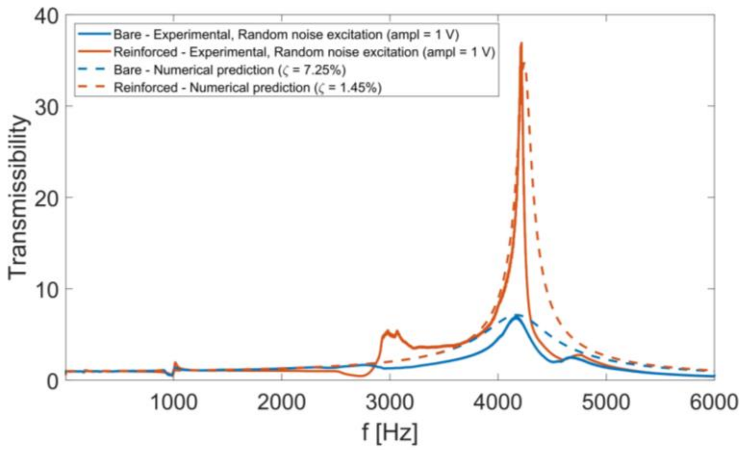

Figure 13: Experimental and numerical results of vibration transmissibility tests. Top mass: 129 gr.

		f [Hz]	A [ ]	η [ ]	K [N/m]	E [MPa]
Bare	Tests	4165	7.01	0.144	9.52e+07	723
	FE	4170	7.13	0.142	9.49e+07	721
Reinforced	Tests	4214	35.7	0.0274	9.82e+07	746
	FE	4240	34.8	0.0287	9.84e+07	747

Table 2: OOP vibration transmissibility: summary of experimental and numerical results.

		η [ ] (Peak Amplitude Method)	η [ ] (Half-Power Method)
Bare	Tests	0.144	0.0586
	FE	0.142	0.145
Reinforced	Tests	0.0274	0.0104
	FE	0.0287	0.0294

Table 3: Loss factor values evaluated by the Peak Amplitude Method and the Half-Power Method.

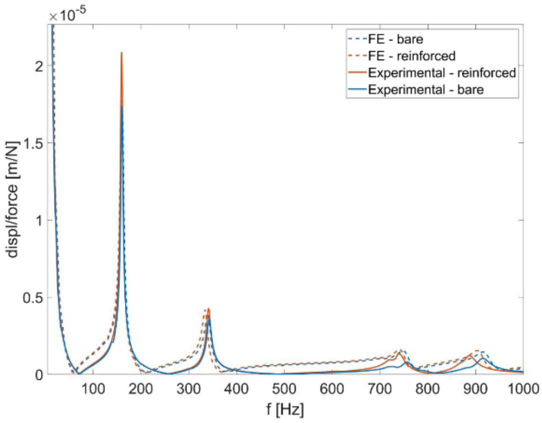

Figure 14: Results of frequency-response simulations and tests on large-scale sandwich panels.

(a)

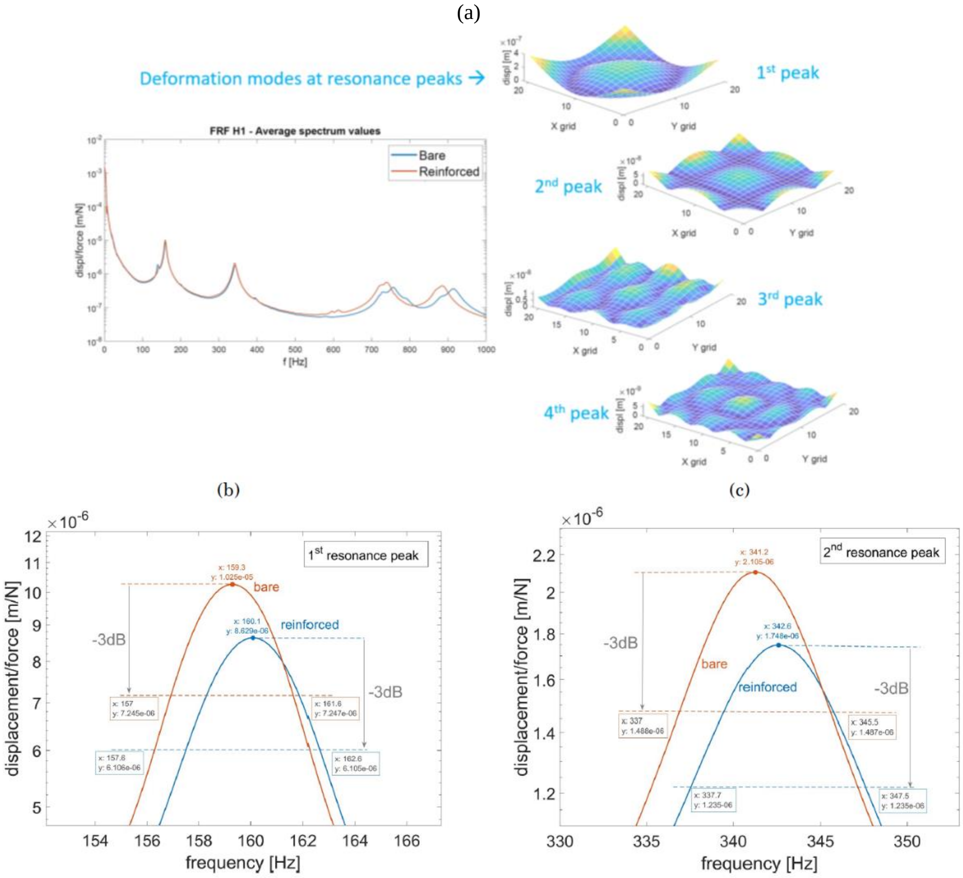

Figure 15: Experimental frequency response: average FRF spectrum with measured deformation modes at resonance peaks. (a) Full spectra; Half-Power Method applied to the first (b) and second (c) peaks.

	Resonance frequency		Loss factor		Inserts contribution to
	Bare	Reinforced	Bare	Reinforced	Damping ratio
1st resonance	159.3 Hz	160.1 Hz	0.0289	0.0312	+8.33%
2nd resonance	341.2 Hz	342.6 Hz	0.0249	0.0286	+15.3%

Table 4: Frequency response measurements on large-scale sandwich panels: damping at the first two resonances of bare and reinforced configurations—Half-Power Method.

ACKNOWLEDGEMENTS

The work was supported by the European Union's Horizon 2020 research and innovation program [Marie Sklodowska-Curie Grant Agreement No. 675441], and the UK EPSRC EP/R032793/1 SYSDYMATS project for materials and testing infrastructure support.

REFERENCES

[1] Z. Xue and J. W. Hutchinson, "A comparative study of impulse-resistant metal sandwich plates," *International Journal of Impact Engineering 30* , pp. 1283-1305, 2004.

[2] F. Cote, V. Deshpande, N. Fleck and A. Evans, "The out-of-plane compressive behaviour of metallic honeycombs," *Materials Science and Engineering: A 380,* pp. 272-280, 2004.

[3] N. A. Fleck and V. S. Deshpande, "The resistance of clamped sandwich beams to shock loading," *ASME. J. Appl. Mech. 71,* pp. 386-401, 2004.

[4] Z. Xue and J. W. Hutchinson, "Crush dynamics of square honeycomb sandwich cores," *International Journal for Numerical Methods in Engineering 65,* pp. 2221-2245, 2006.

[5] A. Hayes, A. Wang, B. Dempsey and D. McDowell, "Mechanics of linear cellular alloys," *Mechanics of Materials 36,* pp. 691-713, 2004.

[6] H. J. Rathbun, D. D. Radford, Z. Xue, M. Y. He, J. Yang, V. Deshpande and e. al., "Performance of metallic honeycomb-core sandwich beams under shock loading," *International Journal of Solids and Structures 43,* pp. 1746-1763, 2006.

[7] A. L. Leao, R. Rowell and N. Tavares, "Applications of natural fibers in automotive industry in Brazil—thermoforming process.," in *Science and technology of polymers and advanced materials (pp.),* Boston, MA, Springer, 1998, pp. 755-761.

[8] M. Karus and M. Kaup, "Natural fibres in the european automotive industry," *Journal of Industrial Hemp,* vol. 7, p. 119–131, 2002.

[9] R. Dunne, D. Desai, R. Sadiku and J. Jayaramudu, "A review of natural fibres, their sustainability and automotive applications," *Journal of Reinforced Plastics and Composites,* vol. 35, pp. 1041-1050, 2016.

[10] M.-A. Boucher, C. Smith, F. Scarpa, R. Rajasekaran and K. Evans, "Effective topologies for vibration damping inserts in honeycomb structures," *Composite Structures,* vol. 106, pp. 1-14, 2013.

[11] F. Scarpa, C. W. Smith, W. Miller, K. Evans and R. Rajasekaran, "Vibration damping structures". United States Patent US9382962B2, 2016.

[12] R. Rajasekaran, M.-A. Boucher, C. W. Smith, F. Scarpa and K. E. Evans, "Vibration damping". United States Patent US9494206B2, 2016.

[13] X. Zhou, E. Shin, K. W. Wang and C. E. Bakis, "Interfacial damping characteristics of carbon nanotube-based composites," *Composites Science and Technology,* vol. 64, pp. 2425-2437, 2004.

[14] H. Rajoria and N. Jalili, "Passive vibration damping enhancement using carbon nanotube-epoxy reinforced composites," *Composites Science and Technology* , vol. 65, pp. 2079-2093, 2005.

[15] G. Barra, L. Guadagno, L. Vertuccio, B. Simonet, B. Santos, M. Zarrelli, M. Arena and M. Viscardi, "Different Methods of Dispersing Carbon Nanotubes in Epoxy Resin and Initial Evaluation of the Obtained Nanocomposite as a Matrix of Carbon Fiber Reinforced Laminate in Terms of Vibroacoustic Performance and Flammability," *Materials,* vol. 12, no. 18, 2019.

[16] Y. Aminanda, B. Castanie, J. J. Barrau and P. Thevenet, "Experimental analysis and modeling of the crushing of honeycomb cores," *Applied Composite Materials,* vol. 12, p. 213–227, 2005.

[17] T. Bitzer, Honeycomb Technology, London SE1 8HN, UK: Chapman & Hall, 1997.

[18] W. Chauvenet, A Manual of Spherical and Practical Astronomy V.II, Lippincott, Philadelphia, 1863.

[19] R. Neville, A. Monti, K. Hazra, F. Scapa, C. Remillat and I. Farrow, "Transverse stiffness and strength of kirigami zero-ν peek honeycombs," *Composite Structures,* vol. 114, pp. 30-40, 2014.

[20] M. Zuhri, Z. Guan and W. Cantwell, "The mechanical properties of natural fibre based honeycomb core materials," *Composites Part B: Engineering,* vol. 58, pp. 1-9, 2014.

[21] A. Stocchi, L. Colabella, A. Cisilino and V. Alvarez, "Manufacturing and testing of a sandwich panel honeycomb core reinforced with natural-fiber fabrics," *Materials & Design,* vol. 55, pp. 394-403, 2014.

[22] S. Del Broccolo, S. Laurenzi and F. Scarpa, "Auxhex – a kirigami inspired zero poisson's ratio cellular structure," *Composite Structures,* vol. 176, pp. 433-441, 2017.

[23] D. I. G. Jones, Viscoelastic vibration damping, Chichester, West Sussex PO19 1UD, England: John Wiley & Sons Ltd, 2001.

[24] A. Savitzky and M. J. E. Golay, "Smoothing and differentiation of data by simplified least-squares procedures," *Analytical Chemistry,* vol. 36, p. 1627–1639, 1964.

[25] C. W. De Silva, Vibration damping, control, and design, CRC Press, 2007.

[26] F. Fahy and P. Gardonio, Sound and Structural Vibration: Radiation, Transmission and Response, Academic Press, second edition, 2007.

[27] J. Halpin, "Effect of environmental factors on composite material design," US Air Force Materials Laboratory, Technical Report AFML-TR 67-423, 1969.

[28] E. Thostenson and T. Chou, "On the elastic properties of carbon nanotube-based composites: modelling and characterization," *Journal of Physics D: Applied Physics,* vol. 36, p. 573–582, 2003.

[29] G. Ghiringhelli, M. Terraneo and E. Vigoni, "Improvement of structures vibroacoustics by widespread embodiment of viscoelastic materials," *Aerospace Science and Technology,* vol. 28, pp. 227-241, 2013.

[30] V. D'Alessanro, G. Petrone, F. Franco and S. De Rosa, "A review of the vibroacoustics of sandwich panels: Models and experiments," *Journal of Sandwich Structures & Materials,* vol. 15, pp. 541-582, 2013.